C6H5Br+· → C6H5 + + Br· occurs via orbiting transition state

3 AUTHORS, INCLUDING:

Sang-hyun Lim
Gwangju Institute of Science and Technology
32 PUBLICATIONS **814** CITATIONS

SEE PROFILE

Joong Chul Choe
Dongguk University
49 PUBLICATIONS **501** CITATIONS

SEE PROFILE

C₆H₅Br⁺• → C₆H₅⁺ + Br• Occurs via Orbiting Transition State

Sang-Hyun Lim,[†] Joong Chul Choe,[‡] and Myung Soo Kim*,[†]

National Creative Research Initiative Center for Control of Reaction Dynamics and Department of Chemistry, Seoul National University, Seoul 151-742, Korea, and Department of Chemistry, University of Suwon, Suwon 440-600, Korea

Received: March 11, 1998; In Final Form: June 26, 1998

Photodissociation of the bromobenzene molecular ion has been investigated on a nanosecond time scale by photodissociation mass-analyzed ion kinetic energy spectrometry. The rate constant and kinetic energy release distribution have been determined. The present experimental data together with the previous milli- to microsecond data have been compared with theoretical calculations. The rate−energy data available over 6 orders of magnitude in time scale could be fit with a nontotally loose transition state model (RRKM) reported by Rosenstock and co-workers. However, the model has been found to predict rate constant values larger than theoretically acceptable at high internal energy. The completely loose transition state model, namely the reaction occurring via orbiting transition state, seems to be a better description of the reaction.

I. Introduction

Dissociation dynamics of polyatomic ions is of fundamental interest in fields such as kinetics, mass spectrometry, cosmochemistry, etc. Various experimental techniques have been developed to measure the rate constant and the product energy partitioning in the dissociation of energy-selected ions.[1−9]

Theoretical development in the area of dissociation dynamics also has been remarkable in recent years.[10−13] Even though the quantum dynamics is thought to be able to provide the most reliable description of a dissociation process,[13] its applicability is limited to 3−4 atom systems at the moment. The classical trajectory calculation which, in principle, can handle more complicated systems[11,14−19] also finds various difficulties in its application to slow (nanosecond or longer lifetime) polyatomic reactions. Hence, the statistical transition state theory, especially the microcanonical Rice−Ramsperger−Kassel−Marcus (RRKM) theory,[20] has been widely applied in the analysis of the experimental data.

The original RRKM theory is particularly useful for a reaction occurring via a tight transition state with a noticeable reverse barrier. In this case, the transition state is usually chosen as a hypersurface passing through the saddle point. Locating the transition state is difficult for reactions occurring with little or no maximum along the minimum energy path, which involve many simple bond cleavage reactions of polyatomic ions. In the extreme case, some of the reactant vibrations may evolve into free rotations (or orbiting motion) in the transition state region. In the phase space theory (PST),[21] the transition state is located at the barrier maximum on the effective potential given by the sum of the long-range attractive interaction between the two fragments and the orbiting kinetic energy. This is called the orbiting transition state (OTS). Due to the assumption of OTS, PST is known to provide an upper bound to the dissociation rate constant.[21d,22] As an intermediate situation, one may suppose the case when the fragment rotation is hindered

at the transition state region. Then, the generalized form of the transition state theory, the variational transition state theory (VTST),[22−24] can be used to calculate the rate constant. Here, the transition state is located based on the variational criterion, namely at the position of the minimum reactive flux. One interesting outcome of the above consideration in recent years is the possible inward movement of the transition state, namely from an OTS to a tight transition state (TTS), as the reactant internal energy increases. This is called the transition state switching.[25−27]

Halogen loss from halobenzene molecular ions (C₆H₅X⁺•, X = Cl, Br, I) has been heavily investigated as prototypes of a reaction occurring via a loose transition state[3,5,27−39]. Recent studies were focused on the possibility of the transition state switching in these reactions.[27,35−39] We also investigated iodine[35] and chlorine[36] losses from C₆H₅I⁺• and C₆H₅Cl⁺•, respectively, using the nanosecond photodissociation kinetics technique[9] developed in this laboratory. It was found that both RRKM and PST provided adequate fits to the experimental data as far as the reaction critical energy was taken as an adjustable parameter. Then, based on the enthalpy of formation of C₆H₅⁺ estimated from independent measurements, it was suggested that RRKM modeling with the use of a tight or nontotally loose transition state was a better description for these reactions.[36] Bromine loss from C₆H₅Br⁺• has received more attention[30,33,34,37−39] than others with regard to the transition state switching. We could not obtain reliable rate−energy data for this reaction, however, due to some experimental difficulties. Recent improvement of the apparatus and availability of a UV laser have removed such difficulties. In this paper, dynamical results obtained for the bromine loss from bromobenzene ion will be presented.

$$C_6H_5Br^{+\bullet} \rightarrow C_6H_5^+ + Br^\bullet \tag{1}$$
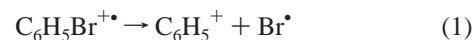
In particular, it will be shown that availability of the rate−energy data on a nanosecond time scale together with the previous micro- to millisecond data helps to elucidate the nature of the transition state involved in this reaction.

---

* Author to whom correspondence should be addressed.
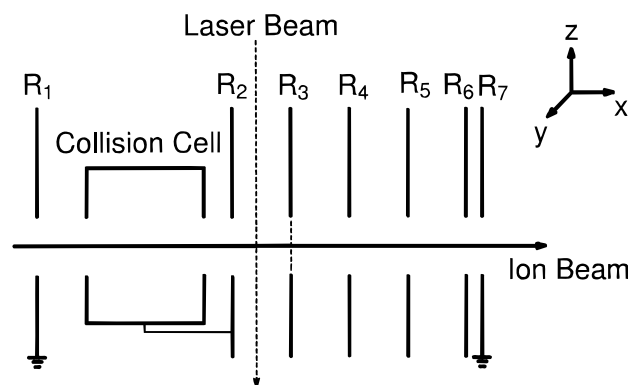† Seoul National University.
‡ University of Suwon.

Figure 1. Schematic diagram of the electrode assembly modified for photodissociation study.

II. Experimental Section

The overall experimental setup was described in detail previously[9,40] and will be reviewed only briefly. Details of the modification made will be presented thereafter. A double-focusing mass spectrometer with reversed geometry (VG Analytical ZAB-E) modified for photodissociation study was used. Molecular ions generated in the ion source at 140 °C by charge exchange using CS_2 as the reagent gas and accelerated to 8 keV were mass-separated by the magnetic sector. Then, the ion beam was crossed perpendicularly with a laser beam inside an electrode assembly (to be described) located near the intermediate focal point of the instrument. The UV-multiple line (mean wavelength of 357 nm) and 457.9 nm line of an argon ion laser (Spectra Physics, BeamLok 2065-7S) and the 488.0 nm line of another argon ion laser (Spectra Physics 164-09) were used. The translational kinetic energy of daughter ions was analyzed by the electric sector. Recording the kinetic energy of daughter ions generated by the dissociation of mass-selected parent ions is called the mass-selected ion kinetic energy spectrometry (MIKES). A MIKE spectrum for photodissociation, or a PD-MIKE spectrum, is usually contaminated by contributions from the same reactions occurring unimolecularly (metastable ion decomposition, MID) or by collision of the parent ions with the residual gas. Hence, phase-sensitive detection using a digital lock-in amplifier (Stanford Research System model SR830) was adopted to record a MIKE spectrum originating only from photodissociation. To improve the quality of a PD-MIKE spectrum, signal averaging was carried out for repetitive scans. Errors quoted in this work were estimated from several duplicate measurements at the 95% confidence limit.

A schematic xz cross section of the electrode assembly used in this work is shown in Figure 1. Here, the x axis is the ion-optical axis, and the z axis is the direction of the magnetic field of the instrument. The collision cell which is normally used for the study of the collision-induced dissociation is just a part of an electrode (R2) in the photodissociation study. Six parallel plate electrodes (R2−R7) have a dimension of 66 mm × 75 mm ($y \times z$) with 0.61 mm thickness. R2, R6, and R7 have 1 mm × 12 mm slits in the center, and R3−R5 have 16 mm × 12 mm apertures. A grid is mounted on R3 to minimize field penetration. The distance between adjacent electrodes of R2−R6 is 1 cm. R1 and R7 are grounded. High voltage can be applied to R2−R6 electrodes independently. Removing R4−R7 and grounding R3, the new design becomes electrically equivalent to the old one.

The fact that high voltages can be applied to R2−R6 electrodes independently allows a few different modes of operation of the electrode assembly. In the voltage-floated
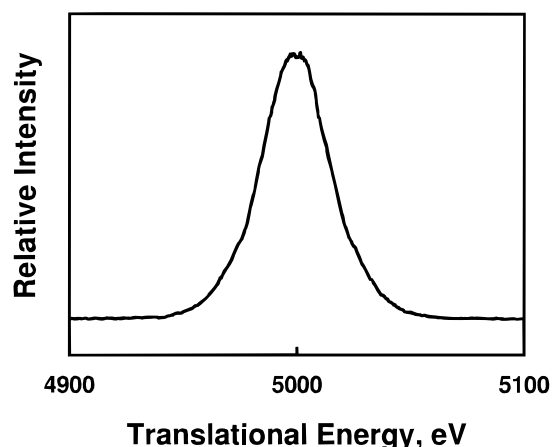

Figure 2. Experimental voltage-floated (2.5 kV) PD-MIKE spectrum for reaction 1 at 357 nm.

mode, R2−R6 electrodes are maintained at the same high voltage. Then, the kinetic energy, after exiting the electrode assembly, of the daughter ion generated in the voltage-floated region becomes different from that of the same daughter ion generated outside the assembly. This results in the separation of these two peaks in the MIKE spectrum. The MIKE profile of the daughter ions generated in the voltage-floated region is used in this work to evaluate the kinetic energy release distribution. Also, this profile is utilized to generate basis functions for the analysis of the time-resolved PD-MIKE profiles. With the previous assembly, the corresponding information was obtained without applying high voltage. The MIKE profile thus obtained, which was called the field-off PD-MIKE profile, usually showed a rather poor signal-to-noise ratio due to the presence of strong MID background. A remarkable improvement in the signal-to-noise ratio with the new design confirmed experimentally enhances the reliability of analysis of the dynamical data.

In the previous design, a high voltage was applied to the R2 electrode such that a constant electric field was present in the dissociation region. Two different modes of operation are possible with the new design. The short-field mode is basically the same as with the old design, a high voltage being applied on R2 and the remainders (R3−R7) being grounded. In the long-field mode, a high voltage is applied on R2 and R6 is grounded. The adjacent electrodes of R2−R6 are connected via 50MΩ resistors such that a constant electric field is present between R2 and R6. Lengthening of the field region allows the rate constant determination on a longer time scale than in the previous design. Utilizing these two modes of time-resolved operation, the rate constant in the range of $1 \times 10^7 - 8 \times 10^8$ s^{-1} can be determined reliably now.

III. Results and Discussion

A. Rate Constant. In the PD-MIKE spectra of bromobenzene ions recorded in this work, the Br loss (reaction 1) was the only dissociation channel. The voltage-floated MIKE spectrum for the photodissociation reaction 1 at 357 nm is shown in Figure 2. A high voltage of 2.5 kV was applied on the electrode assembly to record this spectrum. For a time-resolved PD study, the short-field mode was adopted with the high voltage of 2 kV on the R2 electrode. The time-resolved PD-MIKE spectrum for reaction 1 at 357 nm is shown in Figure 3. The asymmetric tail in the lower-energy side of this profile arises due to time delay between photoexcitation and dissociation. In addition, each profile is broadened due to the kinetic energy release (KER)
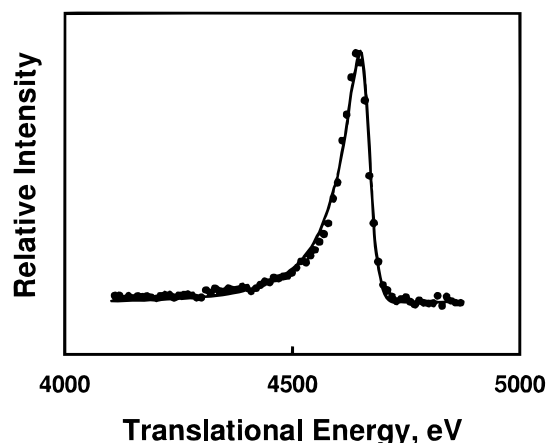
Figure 3. Time-resolved PD-MIKE spectrum at 357 nm for reaction 1 obtained with the short-field mode; 2 kV was applied. Experimental and calculated results are shown as filled circles and a solid curve, respectively.

TABLE 1: Kinetic Energy Releases and Rate Constants for Reaction 1

photodissociation wavelength (nm)	internal energy (eV)[a]	av KER (eV)	rate constant (s^{-1})
488.0	3.76	0.107 ± 0.010	[b]
457.9	3.93	0.116 ± 0.015	(4.8 ± 2.3) × 10^6
357	4.69	0.159 ± 0.015	(2.1 ± 0.5) × 10^8

[a] Estimated with eq 2. [b] Too slow to determine with the present technique.

or its distribution (KERD) in the dissociation step. The method to determine the PD rate constant or its distribution by analyzing a time-resolved PD-MIKE profile was described in detail previously.[9,35,36] The voltage-floated PD-MIKE profile is used to deconvolute the KER broadening in the time-resolved profile. In the case of the time-resolved profile in Figure 3, the most probable rate constant determined by the analysis was 1.3 × 10^8 s^{-1}. From the best-fit rate constant distributions determined by the analysis, the time-resolved PD-MIKE profiles were calculated. The result is included in Figure 3 as a solid line. It was observed for reaction 1 that the rate constant decreased a little bit as the ion source pressure increased. Namely, the collisional relaxation of the molecular ion generated by charge exchange decreased its internal energy, which in turn resulted in the decrease of the observed rate constant. Following the procedure developed previously,[35] the collisional relaxation-free rate constant was estimated by extrapolating the high-pressure data to the zero-pressure limit. The PD rate constant at 357 nm thus determined is (2.1 ± 0.5) × 10^8 s^{-1} for reaction 1 as summarized in Table 1. Also included in the table is the PD rate constant at 457.9 nm determined from the experiment with the long-field mode. The fact that this is a little bit smaller than can be determined reliably resulted in a larger random error. The PD rate at 488.0 nm could not be determined reliably even when the long-field mode was employed. At this wavelength, the rate constant for reaction 1 estimated from the rate−energy data (vide infra) is about 1.5 × 10^6 s^{-1}, which is too small to be determined reliably with the present technique.

The internal energy of a molecular ion generated by charge exchange and then photoexcited can be estimated by the following equation provided that the collisional relaxation is not involved.

$$E = RE - IE + E_{th} + h\nu \qquad (2)$$

Here, RE is the recombination energy of $CS_2^{+\bullet}$ and IE is the ionization energy of bromobenzene. Their best literature values are 10.07 and 8.98 eV, respectively.[41] E_{th} is the thermal internal energy at 140 °C, and its distribution was calculated with the parameters in ref 42 as previously done.[9] The most probable thermal vibrational energy of $C_6H_5Br^{+\bullet}$ at 140 °C was 0.13 eV. Then, the average total internal energy of $C_6H_5Br^{+\bullet}$ photoexcited at 357 nm is 4.69 eV.

The rate−energy relation for reaction 1 has been investigated extensively with various experimental methods on the micro- to millisecond time scale.[27,28,30,33,43−47] These include photo-electron−photoion coincidence spectrometric studies by Rosenstock and co-workers[28] and by Baer and Kury,[43] photoionization studies by Pratt and Chupka,[30] and time-resolved photoionization studies by Malinovich and co-workers.[27,33] RRKM modeling for the halogen loss from halobenzene ions was studied extensively by Rosenstock and co-workers.[3,28] In their most realistic model, the C−X stretch mode was taken as the reaction coordinate and the frequencies of the five remaining halogen-dependent vibrations in the reactant ion were adjusted in the transition state to reproduce the experimental rate−energy data. The best fit to the experimental data with this modeling resulted in the critical energy (E_0) of 2.76 eV and the entropy of activation ($\Delta S^\ddagger$) at 1000 K of 8.07 cal mol^{-1}K^{-1} [48] for reaction 1. Both these values of critical parameters and the method for RRKM calculation have been widely adopted by other investigators.[33,43,47] It is important at this point to mention that Pratt and Chupka[30] noted that a decent fit to the experimental data was also possible with the orbiting transition state (OTS) model when the critical energy was adjusted to a slightly higher value than the above.

RRKM calculation has been extended here to higher internal energy than reported previously, following the same strategy as adopted by Rosenstock and co-workers.[3,28]

$$k(E) = \sigma \frac{W^\ddagger(E - E_0)}{h\rho(E)} \qquad (3)$$

Here, ρ is the density of states of the reactant, $W^\ddagger$ is the state sum at the transition state, and σ is the reaction path degeneracy. Rosenstock and co-workers[28] and other investigators[27,30,33,43] used the experimental vibrational frequencies of the neutral C_6H_5Br[49] in the calculation. Recently, Klippenstein reported the vibrational frequencies of halobenzene ions, $C_6H_5X^{+\bullet}$ (X = F, Cl, Br), calculated by Hartree−Fock (HF) and density functional theory (DFT) methods.[42] For $C_6H_5F^{+\bullet}$ and $C_6H_5Cl^{+\bullet}$, the vibrational frequencies calculated by DFT at the B3LYP/cc-pVDZ′ level display better agreement with the experimental data than the HF results. Accordingly, the vibrational frequencies obtained at the B3LYP/cc-pVDZ′ level by Klippenstein[42] have been used for calculations throughout this work. These are listed in Table 2. Following Rosenstock and co-workers,[28] E_0 of 2.76 eV was adopted and the frequencies of the five bromine-dependent vibrations were adjusted to fit the experimental rate−energy data. A good fit was achieved with $\Delta S^\ddagger$ of 8.07 cal mol^{-1} K^{-1}, which is the same as the one resulting from the analysis of Rosenstock and co-workers. The rate−energy curve thus obtained is shown in Figure 4 together with the previous milli- to microsecond and present nanosecond experimental data. From the figure, it is obvious that the RRKM modeling provides an excellent fit to the experimental data spanning nearly 6 orders of magnitude in time scale.

As was mentioned earlier, it has been known that the experimental rate−energy data for the halogen loss reactions

TABLE 2: Molecular Parameters Used in the Calculations of Rate Constants, KERDs, and Internal Energy Distribution

	vibrational frequencies (cm⁻¹)
$C_6H_5Br^{+\bullet}$ (reactant ion)[a]	3213 3211 3202 3198 3188 1634 1517 1450 1423 1380 1284 1202 1147 1101 1035 1014 1005 997 969 815 783 621 411 363 1072 685[b]547 333 259[c]136[c]
$C_6H_5Br^{+\bullet}$ (TTS)[d]	3213 3211 3202 3198 3188 1634 1517 1450 1423 1380 1284 1202 1147 1101 1035 1014 1005 997 969 815 783 621 411 363 130 130 129 129 129
$C_6H_5^+$ (OTS)[e]	3223 3219 3203 3164 3162 1804 1490 1483 1349 1276 1178 1128 1092 1074 996 987 974 935 893 851 700 652 538 464 414 394 385

	rotational constants (cm⁻¹)
$C_6H_5Br^{+\bullet}$[f]	0.056
$C_6H_5^+$[f]	0.160

	polarizability (10^{-24} cm³)
$Br^{\bullet}$[g]	3.05

[a] Density functional theory calculation on the B3LYP/cc-pVDZ′ level in ref 42. [b] Assumed reaction coordinate in RRKM calculation. [c] Assumed transitional modes in VTST calculation.[27] [d] Transition state frequencies in RRKM calculation. [e] Density functional theory calculation on the B3LYP/6-31G* level in ref 42. [f] MP2/6-31G* estimates in ref 42. [g] From ref 58.
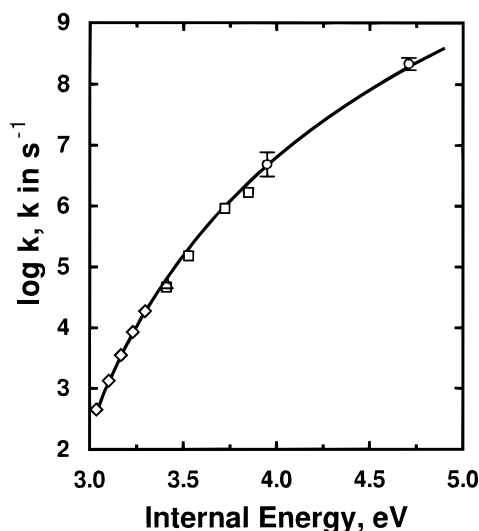

Figure 4. Rate−energy dependence data for reaction 1 reported by (□) Baer and Kury,[43] and by (△) Pratt and Chupka.[30] Present results are shown as circles (○). Solid curve is the reproduction of the RRKM calculation for reaction 1 using $E_0 = 2.76$ eV and $\Delta S^{\ddagger} = 8.07$ cal mol⁻¹ K⁻¹. This is essentially the same as the original RRKM modeling by Rosenstock and co-workers.[28] Also, the original RRKM modeling was reported to provide a good fit to the photoionization efficiency data on a millisecond time scale.[33] To emphasize this point, diamonds (◇) are drawn to indicate the internal energy range covered in the latter experiments.

of halobenzene ions can be interpreted as reactions occurring via either nontotally loose or completely loose transition states.[30,34−36] Rosenstock and co-workers[28] calculated a hypothetical unimolecular thermal A factor from their RRKM fitting of reaction 1 and suggested that the reaction does not occur via an OTS. On the other hand, Lifshitz et al.[7,33] observed that their $\Delta S^{\ddagger}$ recalculated from the original RRKM modeling by Rosenstock and co-workers was very close to the OTS value calculated by Pratt and Chupka[30] using the Klots model[21b,c] of the phase space theory. This led them to conclude that the reaction occurred via a totally loose complex, namely OTS. It
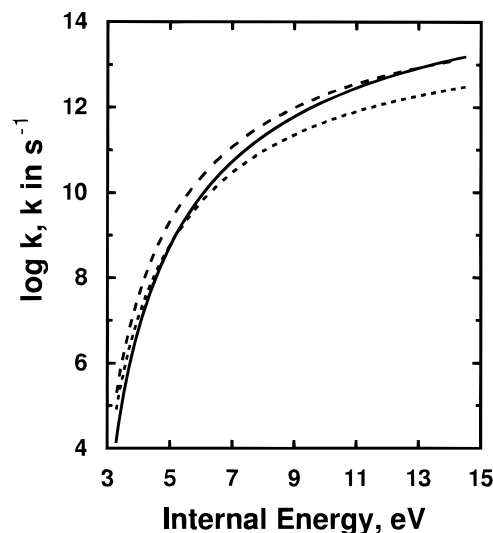

Figure 5. Rate−energy dependence for reaction 1: RRKM calculation (—) with $E_0 = 2.76$ eV and $\Delta S^{\ddagger} = 8.07$ cal mol⁻¹ K⁻¹. PST calculations with $E_0 = 2.76$ eV using frequencies in Table 2 (− − −), phenyl frequencies from Jarrold et al.[25b] (- - -). In all calculations, the frequencies for reactant are taken from Table 2.

is to be pointed out, however, that RRKM is basically a tight transition state model and hence complete looseness of a transition state cannot be judged on the basis of $\Delta S^{\ddagger}$ obtained by an RRKM modeling. In addition, there is some ambiguity in the evaluation of $\Delta S^{\ddagger}$ because the rotational contribution cannot be calculated reliably. In this regard, it is preferable to compare the rate−energy data rather than $\Delta S^{\ddagger}$ values.

The phase space theory calculation of the rate−energy relation of reaction 1 was carried out in this work using the following equation[21d,f] with the TSTPST program[50] developed by Chesnavich and co-workers.

$$k(E,J) = S\frac{\int \rho_v(E - E_o - E_{tr})\,\Gamma_{ro}(E_{tr},J)\,dE_{tr}}{h\rho(E,J)} \quad (4)$$

where

$$\Gamma_{ro}(E_{tr},J) = \int\int\Gamma(E_r^*,J_r)\,dJ_r dL \quad (5)$$

S is the symmetry number ratio of reactant to products, ρ_v is the product vibrational state density, E_{tr} is the product translational energy sum, ρ is the reactant state density, J_r is the total rotational angular momentum quantum number, and Γ is the rotational state sum at total rotational energy less than or equal to E_r^*. J is the angular momentum, and L is the orbital angular momentum. $k(E)$ was obtained by averaging eq 4 with the rotational thermal distribution.[21d] Vibrational frequencies of $C_6H_5Br^{+\bullet}$ and $C_6H_5^+$ obtained at the B3LYP level by Klippenstein[42] were used in the calculation. These and other molecular parameters used are listed in Table 2.

The PST rate−energy curve calculated at 298K with the critical energy (E_0) of 2.76 eV is compared with the above RRKM curve in Figure 5. The temperature dependence of the PST rate−energy curve is very weak and is not important in the present analysis. The experimental rate constants well represented by RRKM are lower than the PST ones by more than an order of magnitude near the reaction threshold, even though discrepancy decreases as the internal energy increases. Hence, PST is not a good description of reaction 1 if an E_0 of 2.76 eV is used. According to VTST, the rate constant of a simple bond cleavage near the threshold is close to the PST

$C_6H_5Br^{+\bullet} \rightarrow C_6H_5^+ + Br^\bullet$

J. Phys. Chem. A, Vol. 102, No. 38, 1998 **7379**

one and becomes smaller than the latter as the internal energy increases (vide supra, see also refs 27, 35–37, 51). The trend predicted from VTST is opposite to that in the experimental data. Hence, if an E_0 of 2.76 eV is used, VTST cannot provide an adequate description of the experimental rate–energy data either. A surprising observation in Figure 5 is that the two theoretical curves, RRKM and PST, cross and the RRKM rate constant becomes larger than the PST one at high internal energy. This is disturbing because the rate constant evaluated at OTS by PST is an upper bound to the actual rate constant as can be understood based on the variational criterion. This suggests a possibility that the RRKM modeling, even though it provided an excellent fit to the experimental data, is not theoretically acceptable in the present case. Or, the vibrational frequencies at the transition state must have been lowered too much in the RRKM modeling.

Since the vibrational frequencies used can affect the calculated rate–energy relation, we repeated the above calculations using other sets of frequencies available from the literature.[21b,25b,49] As was mentioned earlier, the RRKM rate–energy relation was hardly affected by the vibrational frequencies of $C_6H_5Br^{+\bullet}$. For the PST calculation, we used two sets of $C_6H_5Br^{+\bullet}$ frequencies, Klippenstein's[42] and Rosenstock's.[28] Also, three sets of $C_6H_5^+$ frequencies were tested, namely those calculated at the B3LYP and MP2 levels by Klippenstein[42] and the set reported earlier by Jarrold et al.[25b] The PST rate constant was found to be affected noticeably by the vibrational frequencies of $C_6H_5^+$, displaying nearly an order of magnitude difference in the high internal energy region (Figure 5). Regardless, the crossing between the RRKM and PST rate–energy curves was observed in all the cases. We even reduced all the $C_6H_5^+$ vibrational frequencies to 95% of those in Table 2. Crossing still occurred. This leads to the following conclusions. First, the PST with E_0 of 2.76 eV is not an adequate description of the reaction as mentioned earlier. Second, the RRKM modeling is not theoretically acceptable, even though it provides a good fit to the experimental data up to 4.7 eV of the internal energy. It is to be recalled that the good fit with the RRKM modeling was achieved by arbitrarily adjusting some vibrational frequencies. The fact that a good fit can be achieved despite the theoretical deficiency is one of the major weaknesses of the RRKM modeling, especially for reactions occurring via loose transition states. We also attempted other RRKM modelings such as models I and III reported by Rosenstock and co-workers[3] using E_0 of 2.76 eV. All the successful fits to the experimental data crossed the PST rate–energy curve at high internal energy. This leads one to conclude that none of the statistical theories considered here, i.e., PST, VTST, and RRKM, are adequate to explain the experimental rate data of reaction 1 when an E_0 of 2.76 eV is used. This casts doubt on the validity of 2.76 eV as the E_0 value of reaction 1.

We also compared the PST and RRKM calculations at E_0 of 2.38 eV for the iodine loss reaction from $C_6H_5I^{+\bullet}$ reported previously.[35] When the rate–energy relations were calculated at higher internal energy range than previously covered, a crossing between the PST and RRKM rate–energy curves occurred, just as in the case of reaction 1. Namely, the situation for $C_6H_5I^{+\bullet}$ seems to be entirely the same as for $C_6H_5Br^{+\bullet}$. Even though the situation looks similar, we will not deal with the case of $C_6H_5Cl^{+\bullet}$ here because the dynamical data for $C_6H_5Cl^{+\bullet} \rightarrow C_6H_5^+ + Cl^\bullet$ are likely to be less reliable than those for the above two reactions.

A much better fit of PST to the experimental data is possible by adjusting the E_0 value. The PST rate–energy curve
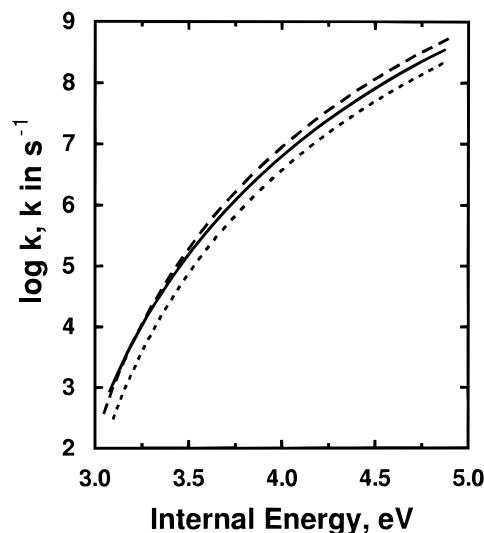

Figure 6. Rate–energy dependence for reaction 1: RRKM calculation (—) with $E_0 = 2.76$ eV and $\Delta S^{\ddagger} = 8.07$ cal mol^{-1} K^{-1}, PST calculation (– – –) with $E_0 = 2.90$ eV at 298 K, and VTST calculation (- - -) following Lifshitz et al.[27] with $E_0 = 2.90$ eV and $a = 3$.

calculated with an E_0 of 2.90 eV is compared with others in Figure 6. We also attempted RRKM calculation with this value of E_0. No successful fit to the experimental data was possible when care was taken such that the RRKM rate did not become larger than the PST one at high internal energy. We also calculated the VTST rate with an E_0 of 2.90 eV and the loosening parameter (a) of 3 following the scheme proposed by Lifshitz et al..[27] One may observe in Figure 6 that the VTST rate constant is a little bit smaller than the experimental or PST ($E_0 = 2.90$ eV) rate constants. The discrepancy between VTST and PST calculations was found, however, to be mainly due to differences in the rotational temperature and different schemes used in the calculations. For example, the VTST calculation displayed good agreement with the PST calculation near 0 K. Such a good agreement between VTST and PST is not surprising, however, because VTST, when a large loosening parameter such as $a = 3$ is used, becomes essentially equivalent to PST.[27] Namely, PST with an E_0 of 2.90 eV seems to be the best description for reaction 1, and the reaction occurs via an orbiting transition state. As was noted earlier, however, the PST rate–energy curve changes as a different set of $C_6H_5^+$ vibrational frequencies is used in the calculation, which requires a change in the value of E_0 to fit the experimental data. For example, an E_0 of 2.85 eV is needed when the frequency set reported by Jarrold et al.[25b] is used in the PST calculation. Both of these values are in better agreement with 2.82 and 2.92 eV calculated at the MP2 and B3LYP levels[42] than 2.76 eV obtained by the RRKM modeling.

The critical energy of 2.90 eV for reaction 1 occurring via OTS allows the evaluation of the enthalpy of formation of $C_6H_5^+$ at 0 K, $\Delta H_f^\circ{}_0$ ($C_6H_5^+$). The thermochemical data needed for the calculation are listed in Table 3. We also refitted the experimental rate–energy data for the iodine loss from $C_6H_5I^{+\bullet}$ reported previously[35] using the PST calculation at 298 K. A decent fit was possible with E_0 of 2.53 eV. As is summarized in Table 3, $\Delta H_f^\circ{}_0$ ($C_6H_5^+$) values obtained by PST fittings of $C_6H_5I^{+\bullet}$ and $C_6H_5Br^{+\bullet}$ data are essentially the same, 1156 kJ mol^{-1}. Also, it is to be mentioned that use of the $C_6H_5^+$ vibrational frequency set reported by Jarrold et al.[25b] for the PST fitting of the above rate–energy data results in $\Delta H_f^\circ{}_0$ ($C_6H_5^+$) of 1151 kJ mol^{-1}, which is in good agreement with 1148 kJ mol^{-1} obtained by Lifshitz and co-workers.[27] In our

TABLE 3: Thermochemical Data (kJ mol^{-1})^a

	C_6H_5X	
	X = Br	X = I
E_0		
TTS	266.3 (2.76)^b	229.6 (2.38)^c
OTS	279.8 (2.90)^d	244.1 (2.53)^d
$\Delta H_f^\circ{}_{298}$ (C_6H_5X)	105.4 ± 4.2^e	164.9 ± 5.9^f
$\Delta H_f^\circ{}_0$ (C_6H_5X)	127.6 ± 4.2^g	180.9 ± 5.9^g
IE (C_6H_5X)	866.4 ± 1.9^e	838.0^e
$\Delta H_f^\circ{}_0$ ($X^\bullet$)	117.9^e	107.2^e
$\Delta H_f^\circ{}_0$ ($C_6H_5^+$)^h		
TTS	1142	1141
OTS	1156	1156

^{a} Numbers in the parentheses are given in eV. ^{b} Ref 28. ^{c} Ref 35. ^{d} This work. ^{e} Ref 41. ^{f} Ref 34. ^{g} Calculated from the room-temperature value using the statistical method described in ref 59. ^{h} Calculated from the values given in this table.

previous studies,[35,36] the value of $\Delta H_f^\circ{}_0$ ($C_6H_5^+$) was taken as an important criterion to judge the validity of the rate models employed. Since $\Delta H_f^\circ{}_0$ ($C_6H_5^+$) evaluated from the ionization energy of $C_6H_5^\bullet$ determined by photoionization[52] and the enthalpy of formation of the same radical obtained from a kinetic experiment[53] was 1125 ± 18 kJ mol^{-1} (use of the more recent $\Delta H_f^\circ{}_0$ ($C_6H_5^\bullet$) datum[54] raises this to 1134 ± 12 kJ mol^{-1}), the OTS model was regarded to be less likely than the tight (or nontotally loose) transition state model. Nicolaides et al.[55] reviewed the problems related to the energetics of $C_6H_5^+$ recently and suggested 1146 kJ mol^{-1} as the best theoretical value for $\Delta H_f^\circ{}_0$ ($C_6H_5^+$), which is a little bit lower than found in the present analysis.

B. Kinetic Energy Release Distribution. Not only the rate−energy relation but also the kinetic energy release (KER) or its distribution (KERD) is known to provide invaluable information on the dissociation dynamics of polyatomic ions. A recent article by Lorquet[56] presents a comprehensive review on this subject. The method to evaluate the KERD from a voltage-floated PD-MIKE profile such as in Figure 2 is well-established now.[57] Since the experimental KERD was rather insensitive to the ion source pressure, it was not necessary to correct for the collisional relaxation effect. Even though it was difficult to obtain the PD rate constant at 488.0 nm, the KERD at the same wavelength could be determined reliably. The KERDs at 488.0, 457.9, and 357 nm are shown in Figure 7. The average KERs evaluated from the distributions are 107, 116, and 159 meV for PDs at 488.0, 457.9, and 357 nm, respectively. The results are summarized in Table 1.

The PST calculations[21d,e] of KERDs have been carried out here using the molecular parameters in Table 2. A critical energy of 2.90 eV has been used. The KERD at each internal energy has been calculated, and averaging over the internal energy distribution arising from the thermal origin has been made. In the cases of PDs at 488.0 and 457.9 nm, the internal energy distribution of the parent ions dissociating inside the voltage-floated region would be different from the overall distribution due to a kinetic reason. This has been corrected for using the RRKM rate−energy curve. KERDs thus evaluated are compared with the experimental data in Figure 7. KERDs calculated by PST agree with the experimental data within error limits, supporting that reaction 1 is indeed a simple bond cleavage with the energy partitioning being determined in the product region.

IV. Conclusions

The rate constant and kinetic energy release distribution in the photoinduced bromine loss from $C_6H_5Br^{+\bullet}$ have been
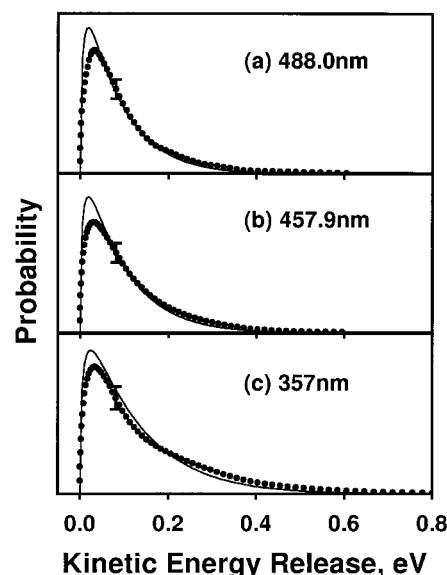

Figure 7. Kinetic energy release distributions for reaction 1: photo-dissociation at (a) 488.0 nm, (b) 457.9 nm, and (c) 357 nm. Experimental results are shown as filled circles. PST calculations are shown as solid curves. Bars represent the error limits.

measured on a nanosecond time scale using the PD-MIKES technique. The rate−energy data thus obtained were in excellent agreement with the extension of the RRKM modeling developed by Rosenstock and co-workers[28] based on similar data obtained on a micro- to millisecond time scale. The PST calculation of the rate−energy relation using the same E_0 value showed, however, that the RRKM rate constant became larger than the PST one at high internal energy. This is a serious problem because the rate constant determined at OTS is supposed to be an upper bound of the actual rate constant according to the variational criterion.[27,30,37] Namely, the RRKM modeling proposed is not valid, even though it provides a good fit to the experimental data. This problem originates from the arbitrariness involved in the conventional RRKM fitting, which is one of the major weaknesses of the method. It is likely that such a difficulty may be a general one rather than an exception for simple bond cleavage reactions occurring via completely or fairly loose transition states. This reasoning is based on the fact that the conventional RRKM theory is basically a tight transition state model which is not adequate for treating very loose transition states. Even though a flexible transition state theory[22,51] is available to deal with such cases, it is difficult to apply to the analysis of experimental data on a routine basis. Hence, carrying out PST calculations of the rate−energy relation and comparing with the experimental and RRKM rate−energy curves as have been done in this work can be of great help in elucidating the dynamical details of a reaction.

It has been found that PST can provide an excellent description of reaction 1 once the critical energy is adjusted slightly upward from the previous value determined by the RRKM modeling. Namely, reaction 1, together with the similar reaction of iodine loss from $C_6H_5I^{+\bullet}$, seems to be a model reaction occurring via a completely loose transition state as was suggested by Lifshitz and co-workers[27] and by Klippenstein.[42] Study of the reaction on an even shorter time scale would be useful to prove or disprove the above conclusion. Analysis of the rate−energy data of reaction 1 based on the OTS model has resulted in $\Delta H_f^\circ{}_0$ ($C_6H_5^+$) which is a little higher than estimated from independent measurements.[52−54] More accurate measurement of this value by independent means would be helpful to confirm the validity of the dynamical model presented

in this work. Also needed is the experimental determination of the vibrational frequencies of $C_6H_5^+$, which have been found to affect the PST rate−energy curve noticeably.

References and Notes

(1) Kühlewind, H.; Kiermeier, A.; Neusser, H. J. *J. Chem. Phys.* **1986**, *85*, 4427.

(2) Baer, T. *Adv. Chem. Phys.* **1986**, *64*, 111.

(3) Rosenstock, H. M.; Stockbauer, R.; Parr, A. C. *J. Chem. Phys.* **1979**, *71*, 3708.

(4) Shin, S. K.; Han, S.-J.; Kim, B. *Int. J. Mass Spectrom. Ion Processes* **1996**, *157/158*, 345.

(5) Stanley, R. J.; Cook, M.; Castleman, A. W., Jr. *J. Phys. Chem.* **1990**, *94*, 3668.

(6) Faulk, J. D.; Dunbar, R. C.; Lifshitz, C. *J. Am. Chem. Soc.* **1990**, *112*, 7893.

(7) Lifshitz, C. *Mass Spectrom. Rev.* **1982**, *1*, 309.

(8) Andlauer, B.; Ottinger, Ch. *Z. Naturforsch.* **1972**, *27A*, 293.

(9) Choe, J. C.; Kim, M. S. *J. Phys. Chem.* **1991**, *95*, 50.

(10) Truhlar, D. G.; Garrett, B. C.; Klippenstein, S. J. *J. Phys. Chem.* **1996**, *100*, 12771.

(11) Rhee, Y. M.; Lee, T. G.; Park, S. C.; Kim, M. S. *J. Chem. Phys.* **1997**, *106*, 1003.

(12) Chen, W.; Hase, W. L.; Schlegel, H. B. *Chem. Phys. Lett.* **1994**, *228*, 436.

(13) Wyatt, R. E.; Zhang, J. Z. *Dynamics of Molecules and Chemical Reactions*; Marcel Dekker: New York, 1996.

(14) Lee, T. G.; Park, S. C.; Kim, M. S. *J. Chem. Phys.* **1996**, *104*, 4517.

(15) Lee, T. G.; Kim, M. S.; Park, S. C. *J. Chem. Phys.* **1996**, *104*, 5472.

(16) Lee, T. G.; Rhee, Y. M.; Kim, M. S.; Park, S. C. *Chem. Phys. Lett.* **1997**, *264*, 303.

(17) Rhee, Y. M.; Kim, M. S. *J. Chem. Phys.* **1997**, *107*, 1394.

(18) Raff, L. M.; Thompson, D. L. *Theory of Chemical Reaction Dynamics;* Baer, M., Ed.; CRC: Boca Raton, FL, 1985; Vol. 3.

(19) Ischtwan, J.; Collins, M. A. *J. Chem. Phys.* **1994**, *100*, 8080.

(20) Robinson, P. J.; Holbrook, K. A. *Unimolecular Reactions*; Wiley: New York, 1972.

(21) (a) Light, J. C. *J. Chem. Phys.* **1964**, *40*, 3221. (b) Klots, C. E. *Z. Naturforsch.* **1972**, *27A*, 553. (c) Klots, C. E. *J. Phys. Chem.* **1971**, *75*, 1526. (d) Chesnavich, W. J.; Bowers, M. T. *J. Am. Chem. Soc.* **1977**, *99*, 1705. (e) Chesnavich, W. J.; Bowers, M. T. *J. Chem. Phys.* **1977**, *66*, 2306. (f) Chesnavich, W. J.; Bowers, M. T. *Gas-Phase Ion Chemistry;* Bowers, M. T., Ed.; Academic Press: New York, 1979; Vol. 1.

(22) Wardlaw, D. M.; Marcus, R. A. *Adv. Chem. Phys.* **1988**, *70*, 231.

(23) Truhlar, D. G.; Garrett, B. C. *Annu. Rev. Phys. Chem.* **1984**, *35*, 159.

(24) Klippenstein, S. J.; Faulk, J. D.; Dunbar, R. C. *J. Chem. Phys.* **1993**, *98*, 243.

(25) (a) Chesnavich, W. J.; Bass, L.; Su, T.; Bowers, M. T. *J. Chem. Phys.* **1981**, *74*, 2228. (b) Jarrold, M. F.; Wagner-Redeker, W.; Illies, A. J.; Kirchner, N. J.; Bowers, M. T. *Int. J. Mass Spectrom. Ion Processes* **1984**, *58*, 63.

(26) Chesnavich, W. J. *J. Chem. Phys.* **1986**, *84*, 2615.

(27) Lifshitz, C.; Louage, F.; Aviyente, V.; Song, K. *J. Phys. Chem.* **1991**, *95*, 9298.

(28) Rosenstock, H. M.; Stockbauer, R.; Parr, A. C. *J. Chem. Phys.* **1980**, *73*, 773.

(29) Dannacher, J.; Rosenstock, H. M.; Buff, R.; Parr, A. C.; Stockbauer, R. L.; Bombach, R.; Stadelmann, J.-P. *Chem. Phys.* **1983**, *75*, 23.

(30) Pratt, S. T.; Chupka, W. A. *Chem. Phys.* **1981**, *62*, 153.

(31) Durant, J. L.; Rider, D. M.; Anderson, S. L.; Proch, F. D.; Zare, R. N. *J. Chem. Phys.* **1984**, *80*, 1817.

(32) Dunbar, R. C.; Honovich, J. P. *Int. J. Mass Spectrom. Ion Processes* **1984**, *58*, 25.

(33) Malinovich, Y.; Arakawa, R.; Haase, G.; Lifshitz, C. *J. Phys. Chem.* **1985**, *89*, 2253.

(34) Malinovich, Y.; Lifshitz, C. *J. Phys. Chem.* **1986**, *90*, 2200.

(35) Yim, Y. H.; Kim, M. S. *J. Phys. Chem.* **1993**, *97*, 12122.

(36) Yim, Y. H.; Kim, M. S. *J. Phys. Chem.* **1994**, *98*, 5201.

(37) Oh, J.; Song, K. *Bull. Korean Chem. Soc.* **1993**, *14*, 404.

(38) Lifshitz, C. *Adv. Mass Spectrom.* **1989**, *11*, 713.

(39) Lifshitz, C. *Int. J. Mass Spectrom. Ion Processes* **1992**, *118/119*, 315.

(40) (a) Choe, J. C.; Kim, M. S. *Int. J. Mass Spectrom. Ion Processes* **1991**, *107*, 103. (b) Choe, J. C.; Kim, M. S. *J. Phys. Chem.* **1992**, *96*, 726.

(41) Lias, S. G.; Bartmess, J. E.; Liebman, J. F.; Holmes, J. L.; Levine, R. D.; Mallard, W. G. *J. Phys. Chem. Ref. Data* **1988**, *17* (Suppl. No. 1).

(42) Klippenstein, S. J. *Int. J. Mass Spectrom. Ion Processes* **1997**, *167/168*, 235.

(43) Baer, T.; Kury, R. *Chem. Phys. Lett.* **1982**, *92*, 659.

(44) Baer, T.; Tsai, B. P.; Smith, D.; Murray, P. T. *J. Chem. Phys.* **1976**, *64*, 2460.

(45) Bouchoux, G. *Org. Mass Spectrom.* **1977**, *12*, 681.

(46) Mruzek, M.; Bouchoux, G. *Int. J. Mass Spectrom. Ion Phys.* **1980**, *33*, 301.

(47) Brand, W. A.; Stocklöv, J.; Walther, H. J. *Int. J. Mass Spectrom. Ion Phys.* **1984**, *59*, 1.

(48) The original value of 8.6 cal mol^{-1} K^{-1} was found to be erroneous in ref 33.

(49) Whiffen, D. H. *J. Chem. Soc.* **1956**, 1350.

(50) Chesnavich, W. J.; Bass, L.; Grice, M. E.; Song, K.; Webb, D. A. *QCPE* **1988**, *8*, 557.

(51) (a) Klippenstein, S. J.; Marcus, R. A. *J. Chem. Phys.* **1989**, *91*, 2280. (b) Klippenstein, S. J.; Marcus, R. A. *J. Chem. Phys.* **1990**, *93*, 2418.

(52) Sergeev, Yu. L.; Akopyan, M. E.; Vilesov, G. I. *Opt. Spektrosk.* **1972**, *32*, 230.

(53) Chen, E. C. M.; Albyn, K.; Dussack, L.; Wentworth, W. E. *J. Phys. Chem.* **1989**, *93*, 6827.

(54) Davico, G. E.; Bierbaum, V. M.; DePuy, C. H.; Ellison, G. B.; Squires, R. R. *J. Am. Chem. Soc.* **1995**, *117*, 2590.

(55) Nicolaides, A.; Smith, D. H.; Jensen, F.; Radom, L. *J. Am. Chem. Soc.* **1997**, *119*, 8083.

(56) Lorquet, J. C. *Mass Spectrom. Rev.* **1994**, *13*, 233.

(57) (a) Yeh, I. C.; Kim, M. S. *Rapid Commun. Mass Spectrom.* **1992**, *6*, 115. (b) Yeh, I. C.; Kim, M. S. *Rapid Commun. Mass Spectrom.* **1992**, *6*, 293.

(58) Lide, D. R. *Handbook of Chemistry and Physics*, *2nd ed.;* CRC: Boca Raton, FL, 1993.

(59) Benson, S. W. *Thermochemical Kinetics*; Wiley: New York, 1976.